Pterodactyl: Effects of 3D Thermal Analysis on Thermal Protection System Design for a Flap Control System

Sarah N. D'Souza,[*] M. Kathleen McGuire,[†]
NASA Ames Research Center, Moffett Field, CA 94035, USA

Andrew Torricelli,[‡] Sander J. Visser,[‡] and
AMA, Inc., NASA Ames Research Center, Moffett Field, CA 94035, USA

Zane B. Hays[§]
STC, Inc., Moffett Field, CA, 94035 Research Assistant, STC, Inc.

NASA's Pterodactyl project has investigated the use of a novel multi-flap control system to facilitate precision targeting of Deployable Entry Vehicles (DEVs) during atmospheric re-entry [1]. DEVs can be folded to fit within the limiting cross-sectional area of current launch systems. Once deployed, the vehicle expands and settles into a pre-determined blunt body shape. While DEVs provide a more efficient solution to increased payload sizes, the absence of a back shell does not allow for easy integration of reaction control systems, which have historically been used for guidance and control (G&C) of rigid aeroshells during entry. One DEV solution, called the Adaptable, Deployable Entry Placement Technology (ADEPT), employs mechanically deployed gores. This provided the Pterodactyl project with the opportunity to incorporate a rib-mounted, 8-flap control system for G&C. Each flap can deflect independently in and out of the hypersonic flow, requiring TPS for the flaps. Previous work within the Pterodactyl project utilized 1D thermal analysis to design the TPS. However, the Pterodactyl project was concerned that the base level tools for 1D thermal analysis were not accounting for the 3D effects of the large heating gradients along and across the flaps, the in-depth in-plane conductivity of the TPS and internal structure, and the effects of the small edge radii at the neck of the flaps. This paper discusses the methodology and results of a 3D thermal analysis of the flap control system. Additionally, the results from the 1D and 3D thermal analyses are compared. It is found that elements of the original design that resulted from the 1D analysis may be overly conservative, and implementation of a 3D thermal analysis indicated a reduction in TPS thickness is feasible. This result helps to reduce the mechanical integration complexity of the flap at the rib tip and realizes potential mass savings.

I. Introduction

NASA's Pterodactyl project has investigated multiple, independent guidance and control (G&C) systems for integration with a mechanically deployed entry vehicle (DEV) to achieve precision targeting [1]. DEVs may accommodate larger payloads which, with the advent of NASA's Moon to Mars program, is becoming critically important to the success of future space missions. Although DEVs provide increased packaging efficiency for large payloads, DEVs lack a back shell which does not allow for easy integration of a traditional reaction control system. Therefore, the Pterodactyl project has developed and analyzed a design that integrates a non-propulsive control system

[*] Principle Investigator, Entry Systems and Vehicle Development Branch, NASA ARC/TSS, AIAA Member.
[†] Aerospace Flight Systems Engineer, Systems Analysis Office, NASA ARC/AA.
[‡] Material Scientist / Engineer, Analytical Mechanics Associates, Inc.
[§] Junior Research Analyst, Systems Analysis Office, NASA ARC/AA, AIAA Member.

with an ADEPT-type (Adaptable, Deployable Entry Placement Technology) entry vehicle, called the Pterodactyl Baseline Vehicle II (PBV-II). PBV-II consists of 8 flaps, mounted at the rib tips of a symmetric, mechanically deployable heatshield, in which each flap can deflect independently in and out of the flow, as shown in Figure 1. As is the case with any novel configuration, an extensive preliminary design process is needed. The Pterodactyl project's preliminary design process consisted of finding a feasible mechanical design, generating an aerodynamic and aerothermal database, developing a trajectory and a guidance and control (G&C) system, and performing preliminary TPS sizing [2]-[10].

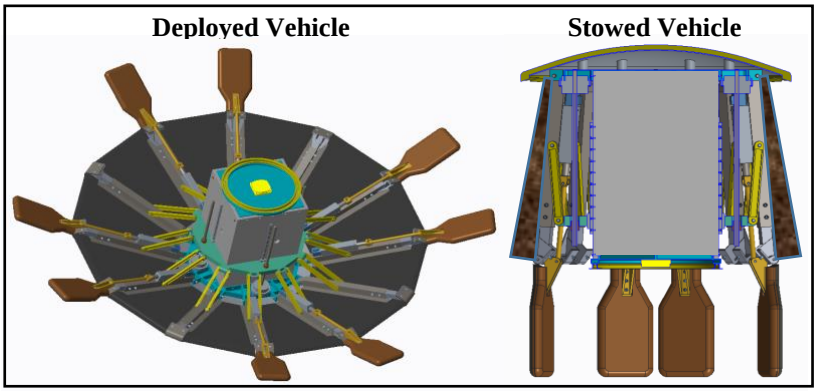

Figure 1:PBV-II re-entry vehicle in a deployed and stowed configuration.

This paper builds upon the findings in Refs. [2]-[10] by conducting an in-depth, 3D thermal analysis for the flap control system. In the initial thermal analysis [6], a couple of issues arose with the initial TPS thickness prediction. First, the initial TPS thickness prediction was such that the total flap thickness (spar plus TPS) was slightly thicker than the rib tip to which it was attached. This result raised potential issues with integrating the actuator hardware, adverse effects to the flap range of motion, and negative effects on the aerodynamics across the flap-rib tip interface. Second, the accuracy of using 1D analysis to size the TPS was an area of concern given the complicated flap geometry. Namely, the concern was whether the tools were capturing the actual hot point on the flap throughout the whole trajectory. Further, the 1D thermal analysis could not capture the 3D effects of the large heating gradients along and across the flaps, the in-depth in-plane conductivity of the TPS and internal structure, and the effects of the small edge radii at the neck of the flaps. Therefore, improvements were made to the TPS Design methodology, found in [6], by increasing the fidelity of the aeroheating environments and the thermal analysis to include 3D effects. This paper focuses on the 3D thermal analysis results, while computation of the higher fidelity aeroheating environments is documented in [9]. Note that the analysis in [9] was used to downselect which flap(s) have the worst-case heating and provide the boundary conditions for the 3D thermal analysis discussed in this paper. The objective of this work is to demonstrate that the inclusion of 3D effects is significant enough to affect the predicted temperatures of the flap, affect the required amount of TPS, and identify whether the PBV-II flap control design is mechanically feasible.

II. Trajectory Specification and Vehicle Geometry

Thermal analysis of this flap configuration requires aerothermal environments as inputs to the analysis. These aerothermal environments are a function of the entry trajectory and vehicle design. Therefore, it is important to detail key aspects of the trajectory and vehicle design to put the results of the thermal analysis in the correct context.

A. Vehicle Configuration

The vehicle configuration is illustrated in Figure 2 and shows how the flaps are arranged around the 2.86m diameter heatshield, in reference to the vehicle coordinate system. PBV-II employs eight flared flaps that rotate about their respective rib tip shoulder. Although a simple rectangular shape would have been preferred to remove heating and TPS complexities, a flap width larger than the ribs was selected to provide sufficient control authority. Thus, the inboard width was tapered down to match the width of the ADEPT rib tips. This allowed the flaps to rotate about the rib tips while avoiding complex aeroshell shoulder geometry adjacent to the rib tips.

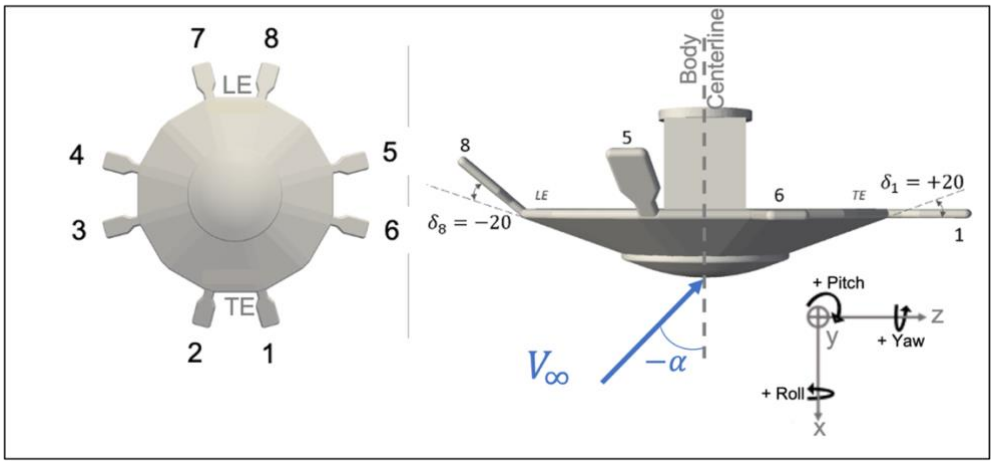

Figure 2: PBV-II flap designations and deflections defined.

The orientation of this low L/D vehicle is such that the vehicle will be Lift vector up at negative angle of attack ($\alpha < 0^o$) and Lift vector down for $\alpha > 0^o$. Therefore, a Lift up orientation ($\alpha < 0^o$) corresponds to the trailing edge (TE) being pushed down, while the leading edge (LE) is pulled up. For more detail on the vehicle and flap mechanical design, see Ref. [1] and [2].

B. Flap Geometry and TPS Material

The high heating and velocities of the trajectory require a flap material capable of withstanding heat rates and pressures both thermally and mechanically. Heatshield for Extreme Entry Environment Technology (HEEET) was chosen for the TPS and details about HEEET are discussed in [11] and [12]. HEEET is adequately suited to withstand high heating environments up to 3600 W/cm^2 [13]. HEEET is a 3D woven carbon fabric infused with a phenolic resin to create a solid that has an outer, dense, Recession Layer (RL) and an inner, less dense, and less conductive, Insulation Layer (IL). In the PBV-II design, HEEET material is wrapped around a titanium spar to form the flap shape, allowing the titanium to add rigidity to the flap structure, Figure 3.

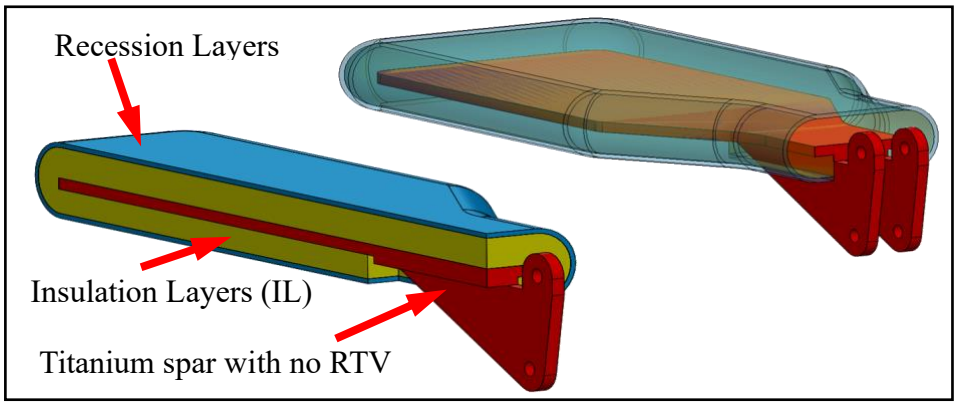

Figure 3: HEEET Flap Design

The titanium spar has a temperature limit which is used as a constraint in the thermal analysis. Two different structural temperature limits were examined i) 589 K, corresponding to the typical allowable temperature for titanium which was used as a preliminary value for the initial study and ii) 900 K, based on the structural assessment of the titanium spar under the PBV-II predicted loading conditions. The spar thickness is included in the analysis to determine thermal mass, conductivity, and soak back. The spar sizing is discussed in [1].

C. Entry Trajectory, Vehicle Attitude, and Flap Deflections

The PBV-II vehicle is designed to perform an Earth entry at lunar return speeds and the selection of this mission concept of operations is discussed in [10] and illustrated in Figure 4.

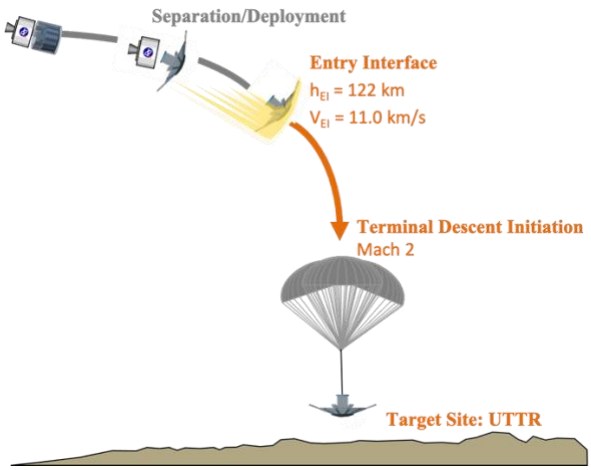

Figure 4: Pterodactyl entry concept of operations

The PBV-II baseline trajectory is shown in Figure 5 and the details of its development are discussed in Ref. [8]. At 400 sec the trajectory terminates because it hits the Mach 2 terminal condition and signifies the end of entry phase. Note that an additional 400 seconds is added to the thermal analysis to account for soak back. The descent and landing phases are not considered in this analysis.

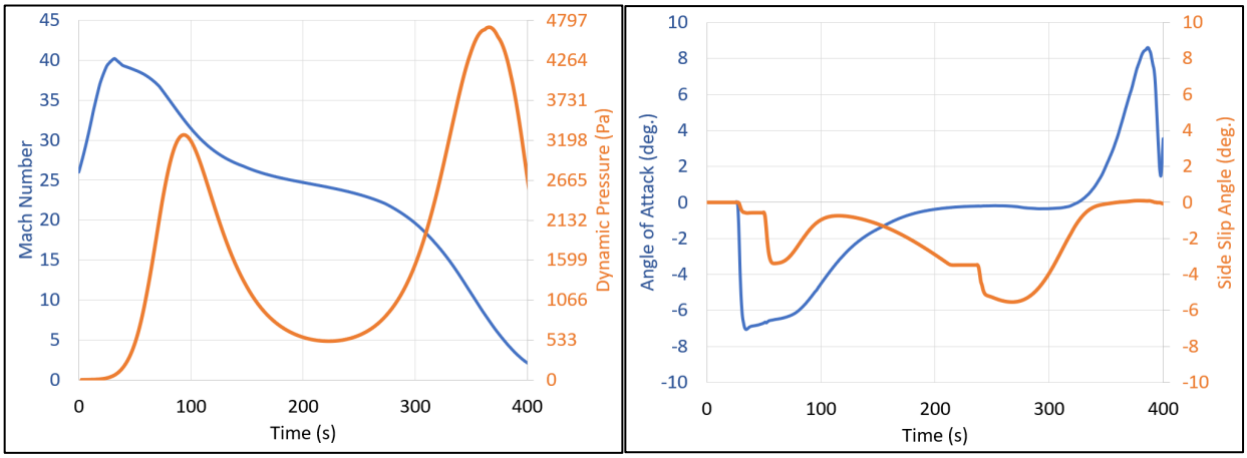

Figure 5: Entry trajectory Mach number and Dynamic Pressure (left) and vehicle α/β guidance commands (right).

Note the double pressure spikes shown in Figure 5 (left, orange). These peaks are due to the vehicle completing a lofted trajectory, which is needed to burn off the energy from high entry speeds to meet the target range requirements. This trajectory characteristic will be important when examining the thermal effects for various flap deflections throughout the trajectory, namely if the flap is deflected into the flow during high velocity and increasing air density conditions. Additionally, the intensity of the aerothermal environment is partially impacted by the overall attitude of the vehicle. In the right plot in Figure 5, note the negative sideslip (β) angle throughout the trajectory and the change in sign on α while in the second dynamic pressure pulse. Due to the negative β, one side of the vehicle is likely to experience higher heating than the other, in this case the side with flaps 2, 3, 4, and 7. A negative α exposes the leading edge of the vehicle such that flaps 1 and 2 are not directly exposed to the flow for much of the trajectory. However, it is expected that if any flap is deflected into the flow during high velocity and increasing dynamic pressure conditions, the heating environments around the flap will go up.

The stability and control analysis discussed in Ref. [8] provides the flap deflection schedule for each flap to track the guidance commands found in Figure 5 (right). The resulting flap deflection schedules are shown in Figure 6 for all eight flaps.

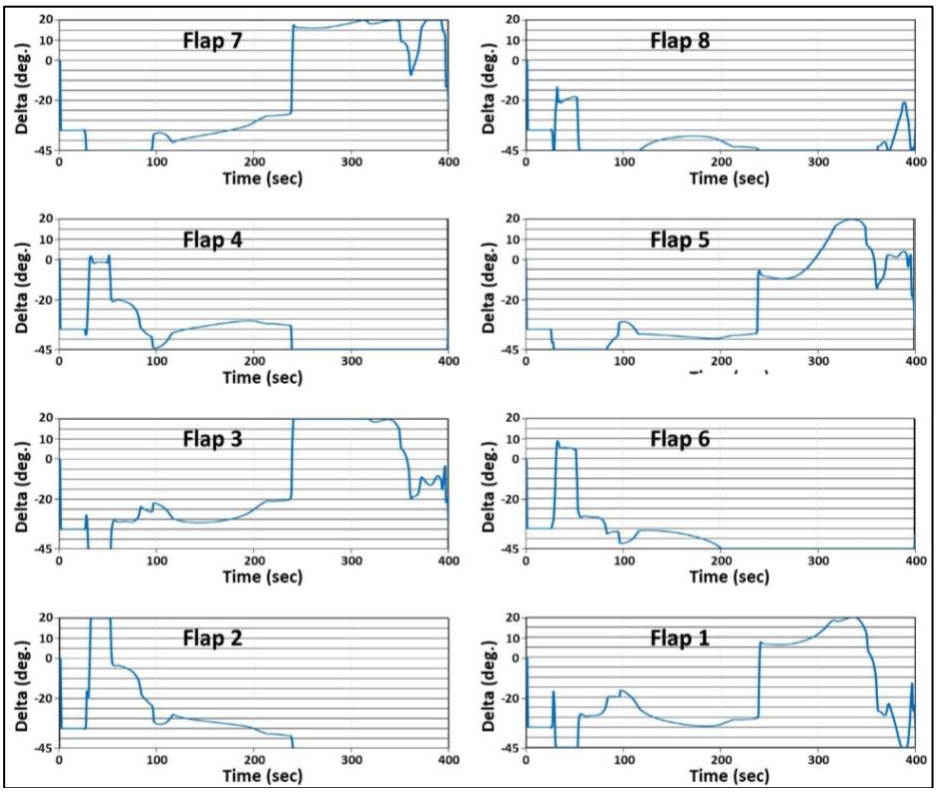

Figure 6: Flap deflection angle schedule.

Notice the change in flap deflections coinciding with the transition of α from negative to positive. Additionally, during the first half of the trajectory the flaps are mostly deflected out of the flow, at $\delta < 0^o$, with a few brief spikes to $\delta > 0^o$. During the second half of the trajectory, flaps 1, 3, 5, and 7 are deflected at large positive angles into the flow for a prolonged amount of time, correlating to the transition of α and β in the latter half of the trajectory.

III. 3D Thermal Analysis Methodology

A. Overview

The thermal analysis for the flap is the fourth phase of an overall TPS Design methodology for the Pterodactyl flap control system. These phases are illustrated in Figure 7. The objective of Phase 4 is to analyze the 3D effects on the heat transfer through the flap and refine the flap TPS thickness. Therefore, the Phase 4, 3D thermal analysis requires a geometry model and a complete set of boundary conditions, which are calculated in [9]. For brevity only the relevant results of the aerothermodynamic and 1D thermal analysis are noted in Section III.D. The 3D thermal analysis uses surface temperature time histories and convective heat rate boundary conditions on the windward and aft side of the flap, respectively ([9]). Additionally, the Phase 3, 1D thermal analysis was used to identify an initial RL and IL thickness for the CAD model needed for the 3D thermal analysis. Finally, a 400 second soak back was added to the end of the trajectory to characterize flap survivability. However, this soak back does not constitute any analysis of the descent or landing phases.

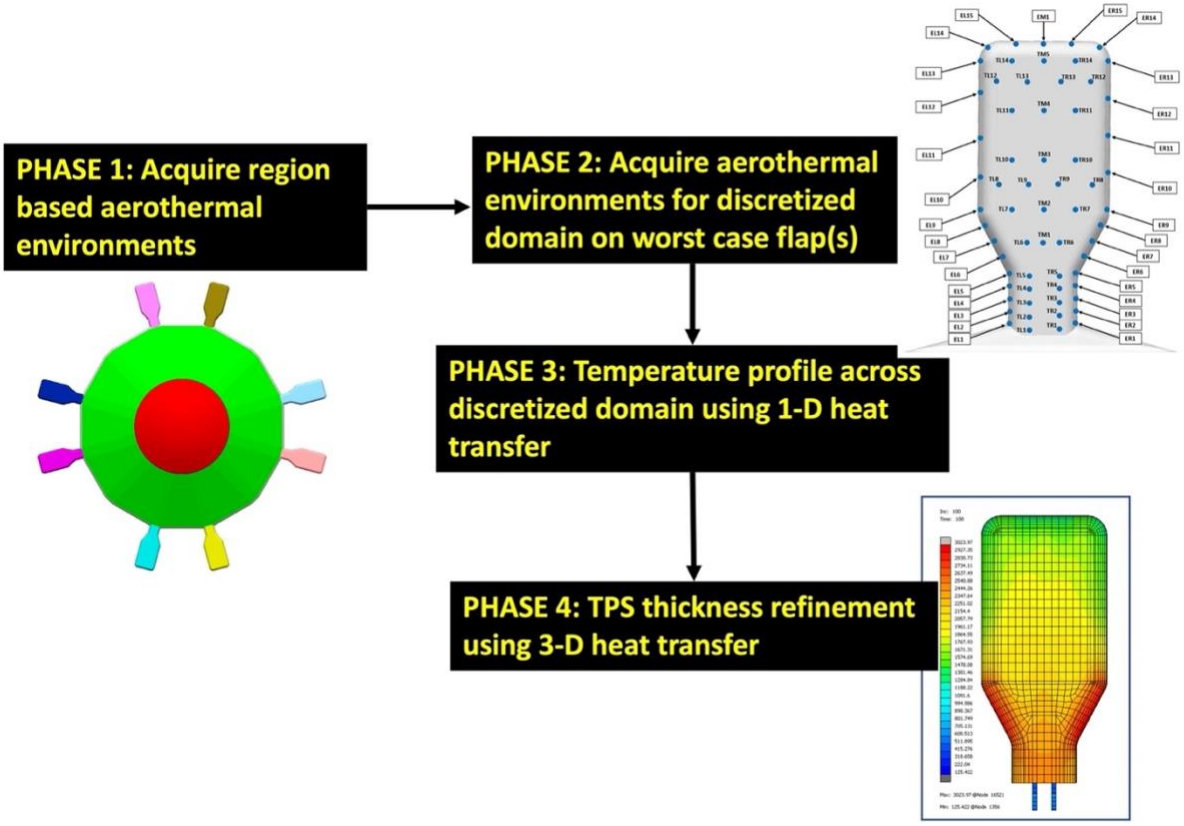

Figure 7: Pterodactyl TPS Design phases

B. Tool Description

The tool used for the 1D Thermal analysis was TPSSizer [14], a tool designed to work with CBAero [15] and FIAT [16] to determine the required TPS thickness at specified sizing points on a vehicle flown through a given trajectory. CBAero predicts the aerodynamic and aero-thermodynamic environments for a given vehicle and FIAT is a 1D thermal analysis code that predicts the temperatures and heat rates through the TPS stack-up. Additionally, TPSSizer calculates the TPS mass and optimizes TPS thickness for both non-ablative and ablative TPS materials, while satisfying the allowable temperature constraints applied to the TPS material stack-up. The 3D thermal analysis in this work was completed using Marc/Mentat [17], which is a nonlinear finite element analysis (FEA) software used to perform 3D heat transfer analysis to acquire temperatures through and across the flaps.

C. Analysis Method Validation

In the final analysis, we will be comparing the results from Marc/Mentat to those from the 1D FIAT analysis. To prepare, a simplified comparison study was completed to ensure proper implementation of the material properties and heat transfer properties in Marc/Mentat as compared to FIAT. It is important to note that Marc/Mentat does not model ablation, but FIAT does. Therefore, for the validation, ablation was turned off in FIAT for the purposes of comparison. The comparison shown in Figure 8 was for a constant 1700 second heat pulse. Models with complex time-dependent heating were equally tested in both programs and the results are in good agreement. Overall, the average error between FIAT and Marc/Mentat temperatures was less than 5%. Having determined that the 1D Marc/Mentat results agree with those obtained from FIAT, the next step is to use the full-scale flap design and build a 3D thermal analysis model in Marc/Mentat.

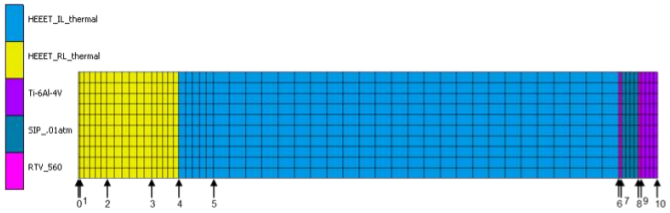

Position	0	1	2	3	4	5	6	7	8	9	10
Pos Depth (cm)	0.000	0.0150	0.269	0.691	0.945	1.270	5.080	5.110	5.263	5.293	5.446
Peak Mentat (°C)	1181.6	1180.1	1148.6	1094.0	1060.0	998.0	483.4	483.1	481.1	480.9	480.9
Peak Fiat (°C)	1163.5	1161.7	1130.4	1076.0	1041.3	980.2	474.3	474.1	472.2	472.0	472.0
Δ Peak Temp (°C)	18.1	18.4	18.2	17.9	18.7	17.8	9.1	9.1	8.9	8.9	8.9

Max Peak ΔTemp (°C)	18.7
Avg Peak ΔTemp (°C)	14.0

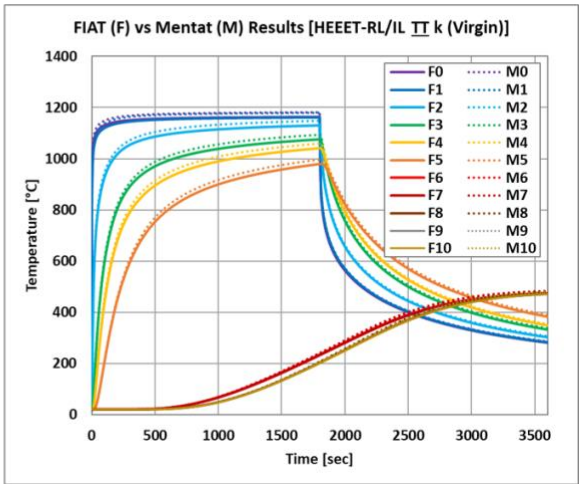

Figure 8: Validation comparison of results from FIAT and Marc/Mentat

D. Flap TPS CAD, Meshing and Boundary Conditions

The flap dimensions for the CAD used in this analysis are depicted in Figure 9. The thickness of Flap 3 was used because it was found to require the most TPS based on the 1D FIAT analysis in [9].

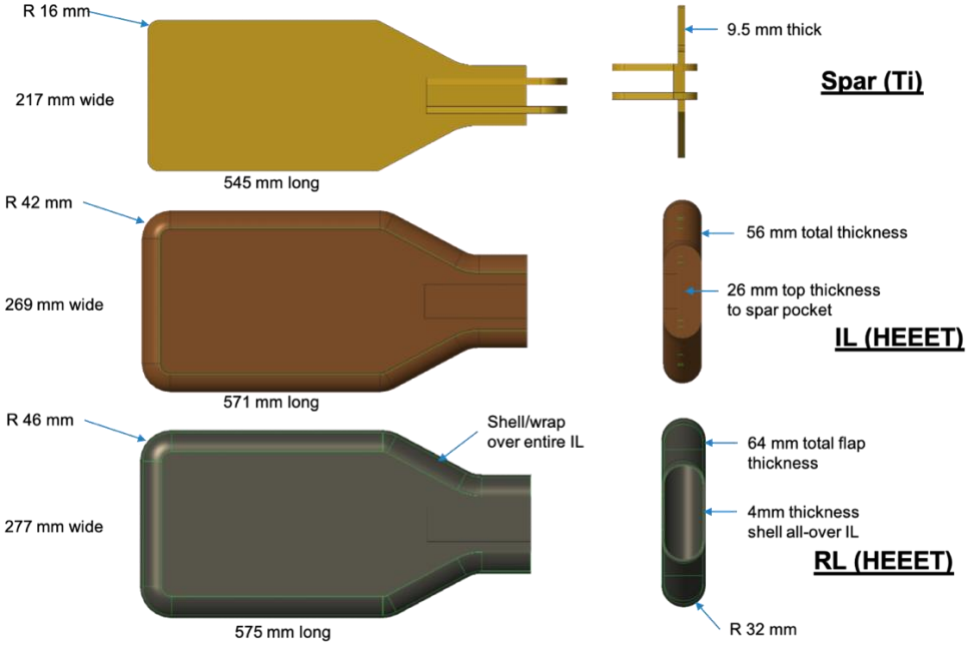

Figure 9: Flap geometry dimensions for FEA.

The 3D flap design was imported into Patran to generate a structured mesh for use in the FEM analysis tool Marc/Mentat. A structured mesh was selected over an unstructured mesh, so that any uniform TPS thickness changes could be accommodated by the removal of a layer of elements. Figure 10(A) illustrates the mesh discretization as well as the areas of mesh refinement. The HEEET RL (blue) and the outer layers of the HEEET IL (yellow) are thinner than the remainder of the HEEET IL and the spar (red) to facilitate thickness removal, simulating recession. The model counts a total of 26,525 nodes and 24,654 quadrilateral elements.

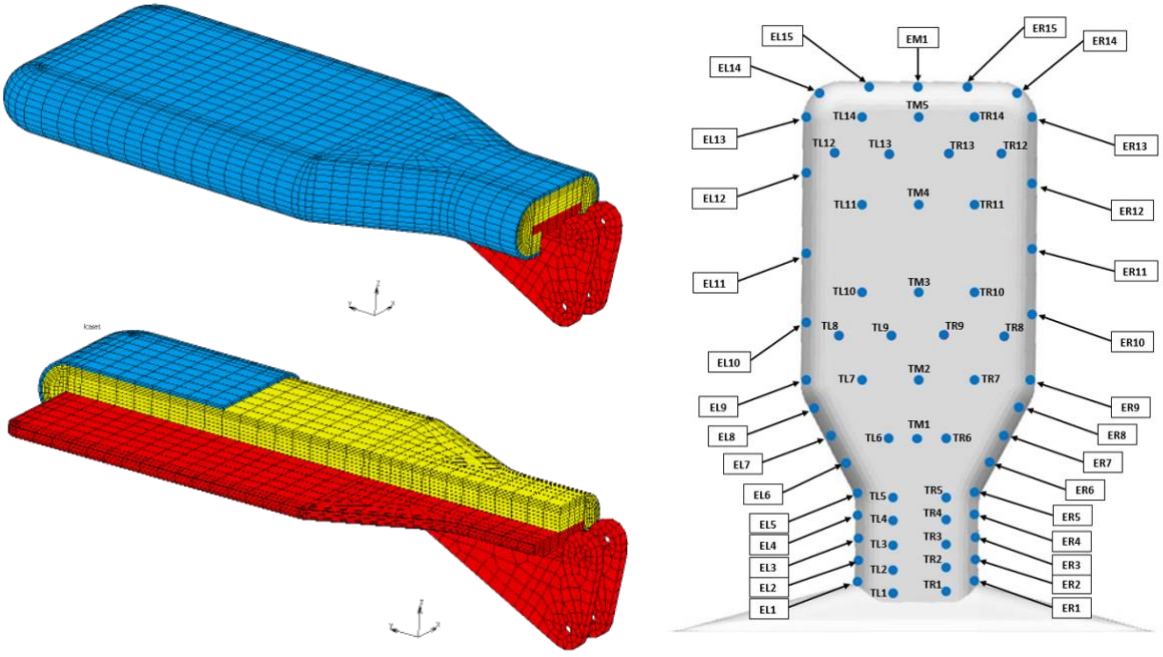

(A) **(B)**

Figure 10: (A) Marc/Mentat windward view of the discretized Titanium spar and bracket (red), HEEET IL (yellow) and HEEET RL (blue), (B) Surface points where the boundary conditions for the 3D thermal analysis are to be applied.

The boundary conditions for this analysis are applied based on the 64 points analyzed in the 1D FIAT analysis completed in [9] and shown in Figure 10(B). The location and spread of the 64 points were determined based on the areas where high pressure and heating were observed in the aerothermal analysis. From the 1D analysis, the resultant temperatures and heat fluxes were linearly interpolated between the 64 data points on a 25x25 grid. This resulted in a 4D map of the temperatures and fluxes with independent variables x, y, & t (time).

To accommodate the fact that Marc/Mentat does not model recession, the recession boundary condition was applied for 2 bounding configurations, one with the Recession Layer (RL) intact and one with the RL removed (Figure 11). In addition, this analysis applies different Through-the-Thickness (TTT) and In-Plane (IP) material properties. The orientation assumes the TTT direction to be towards the center spar (Figure 12).

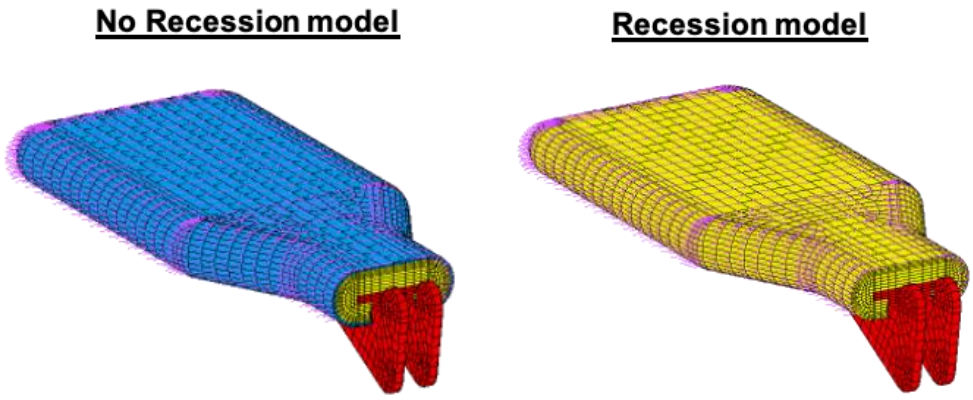

Figure 11: Different cases run in Marc/Mentat, 1) include recession layer (left) and 2) no recession layer (right).

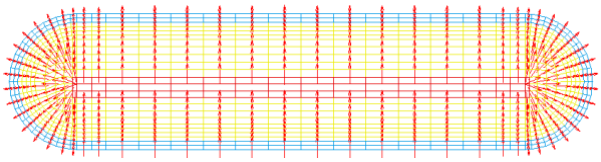

Figure 12: Through the thickness orientation.

An initial temperature of 260.93 K is applied to all nodes and the exterior radiation boundary condition is a 294.26 K sink radiation applied to all exterior surfaces to match the analysis in [9]. A time and location varying temperature boundary condition is applied to the surface nodes on the windward side resulting from the interpolation of the 1D results on the 64 nodes of Flap 3. Figure 13 plots the surface temperatures at select time points in the trajectory to illustrate the temperature boundary conditions applied to the windward side of the flap.

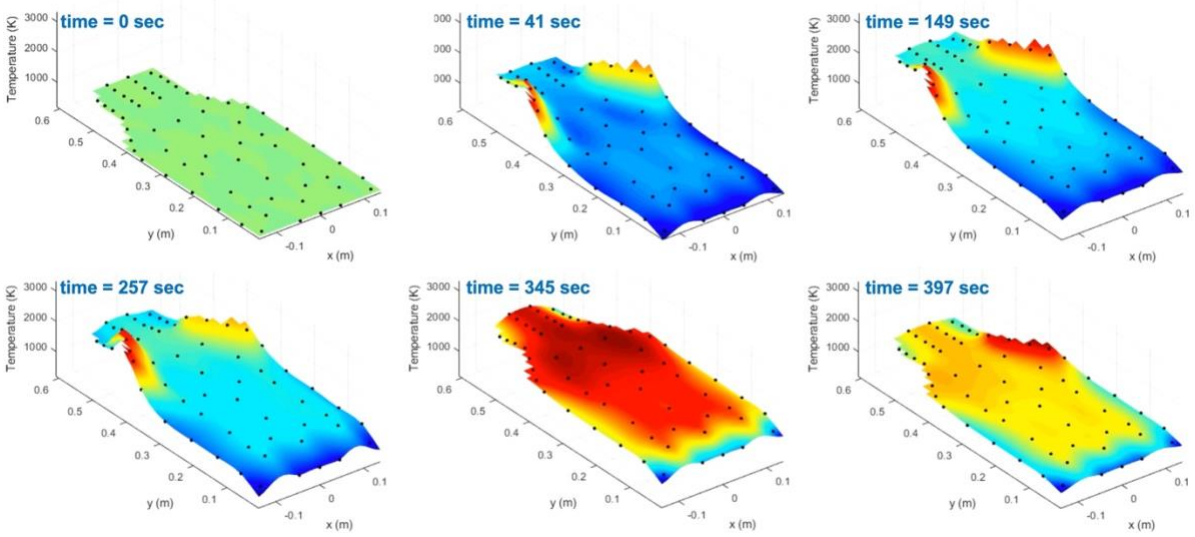

Figure 13: Topographic map of the surface temperature boundary conditions, across the windward side of the flap, at different times in the trajectory

Note that the boundary conditions from [9] do not include surface temperature time histories for the aft side because of wake modeling complexities in the aerothermodynamics computation process [9] and the aft side is not expected to experience recession. Therefore, a conservative ratio, informed by a high fidelity US3D [18] aerothermodynamics simulation [7], was applied to determine the worst case heat rate boundary conditions for the aft side. This ratio is:

$$R_{conv} = \left.\frac{\dot{q}_{\text{aft}}}{\dot{q}_{\text{windward}}}\right|_{US3D} \tag{1}$$

where R_{conv} is a constant ratio of the worst case aft convective heat rate ($\dot{q}_{\text{aft, US3D}}$) to windward convective heat rate ($\dot{q}_{\text{windward, US3D}}$). This ratio was then applied to the surface windward heat rates ($\dot{q}(t)_{\text{windward, phase 3}}$) defined in Phase 3 (Figure 7, [9]) to determine the surface aft heat rates ($\dot{q}(t)_{\text{aft, phase 3}}$):

$$\dot{q}(t)_{\text{aft, phase 3}} = R_{conv} * \dot{q}(t)_{\text{windward, phase 3}} \tag{2}$$

A conservative value of $R_{conv} = 0.10$ was selected and applied to the interpolated windward heat rates. Given the complexity and uncertainties in modeling the recirculating flow on the aft side of the flaps, the choice to use a conservative factor was made to limit the computational scope of the analysis providing the aft environment. The aft heat rates were also applied to the exposed portion of the titanium spar/bracket, since it is expected that the bracket will be experiencing similar heating (Figure 14) and heating directly to the bracket impacts the resulting spar temperatures. For brevity, only the surface temperature profiles are plotted, but the maximum windward side heat rate for flap 3 is 100.8 W/cm^2. Therefore, the heat rate boundary conditions will be up to 10 W/cm^2.

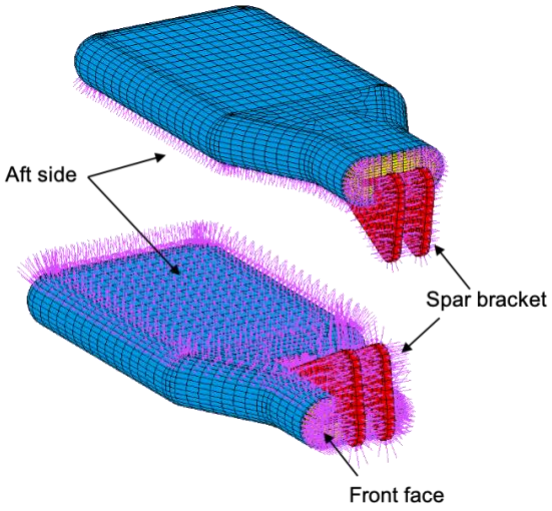

Figure 14: Aft side boundary conditions.

The goal of this analysis is to determine the temperature of the spar over the course of the entry trajectory and compare the 3D temperature predictions to those of the 1D FIAT analyses. If the spar temperature exceeds the thermal limits for the titanium, then this implies that the HEEET IL must be resized from the 1D analysis. However, if the spar temperature is lower than the thermal limits for titanium, then it is possible to reduce the HEEET IL and realize TPS mass savings.

IV. Thermal Analysis Results

Analysis of the titanium spar shows that the temperature first increases at the exposed hinge location. Locations covered by TPS have a delayed response to the outside environment, as heat takes time to move through the TPS. The result is a larger increase in temperatures near the hinge with temperatures slowly spreading towards the outer flap. As the soak back temperature increases, temperature concentrations can be seen near the outer corners and especially at the shoulders (Figure 15).

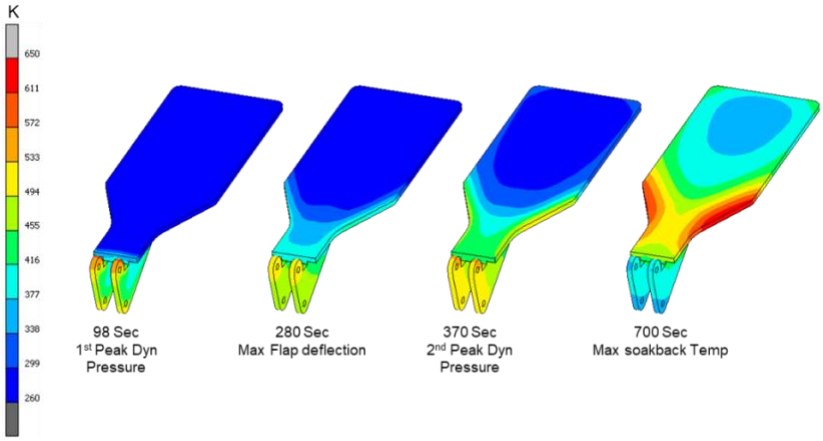

Figure 15: Titanium spar temperatures at various times during the trajectory.

One of the goals of the analysis was to determine the magnitude of 3D effects when switching from a 1D point analysis to a fully 3D analysis. Due to the geometry of the flap, the positioning of the spar within the TPS, and the dynamic heating during entry, 3D effects were to be expected. Figure 16 shows a comparison of the 1D FIAT and 3D Marc/Mentat temperature history predictions for the spar locations directly under a selection of the 64-point locations. For the locations close to the bracket (Points 1-3) the initial temperature rise is faster in the 3D model than the 1D

because the spar is being heated by the exposed bracket. The rates of temperature rise in the locations further away from the bracket (Points 4-7) are slower in the 3D predictions than the 1D. This is possibly due to the in-plane effects and the added thermal mass of the TPS on the aft side of the bracket, which was not modeled in the 1D analysis. Later in the trajectory, most locations show lower temperatures in the 3D analysis compared to the 1D due to the added thermal mass on the aft side of the spar.

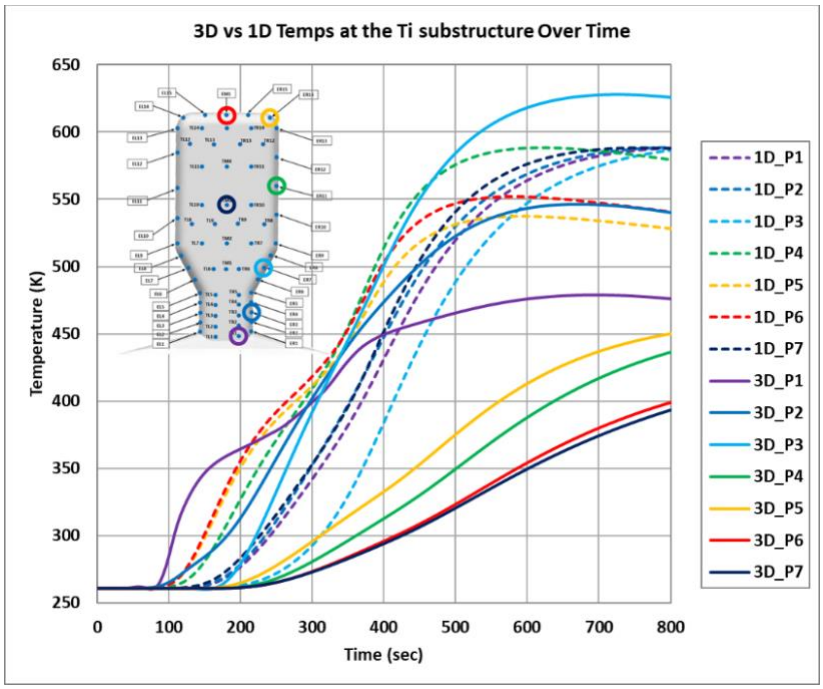

Figure 16: Temperature history comparison of the 1D FIAT and 3D Mentat results at select locations.

By the end of the trajectory, only Point 3 shows a higher temperature concentration in the 3D analysis (Figure 17). This result suggests that it might also be beneficial to the TPS mass if the HEEET thickness could be tapered to be thicker at the spar and thinner outboard, while observing the mechanical constraints at the rib tip attachment point.

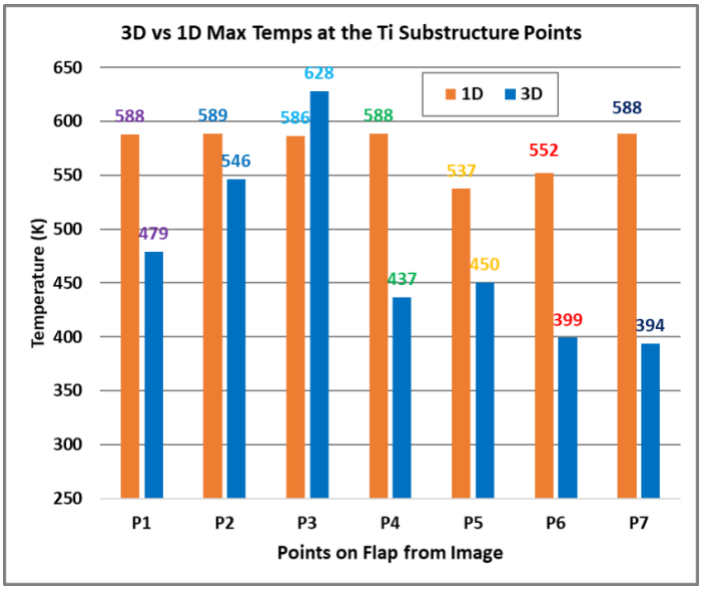

Figure 17: Max temperature comparison of 1D FIAT and 3D Mentat at the locations in (Figure 16)

The FIAT 1D analysis tool can predict material recession and pyrolysis during entry, but does not accurately predict soakback temperatures when 3D effects are present. Due to the inability to model pyrolysis and recession in Marc/Mentat, two bounding cases were analysed at the shoulder, the location of highest temperature concentration. The upper bound case has no recession layer, while the lower bound case has an intact recession layer with no recession or pyrolysis effects. The true peak temperature of the titanium spar is somewhere between these two bounds. The results show that the higher bound max temperature of the spar is still below the lower, typical allowable temperature for titanium at 400 seconds (the end of the entry phase of the trajectory) (Figure 18). Considering temperature soak-back after the end of the trajectory, this approach shows that with 3D effects and recession and pyrolysis effects conservatively removed, the spar is predicted to be well below the higher titanium allowable temperature coming out of the structural analysis (Figure 18).

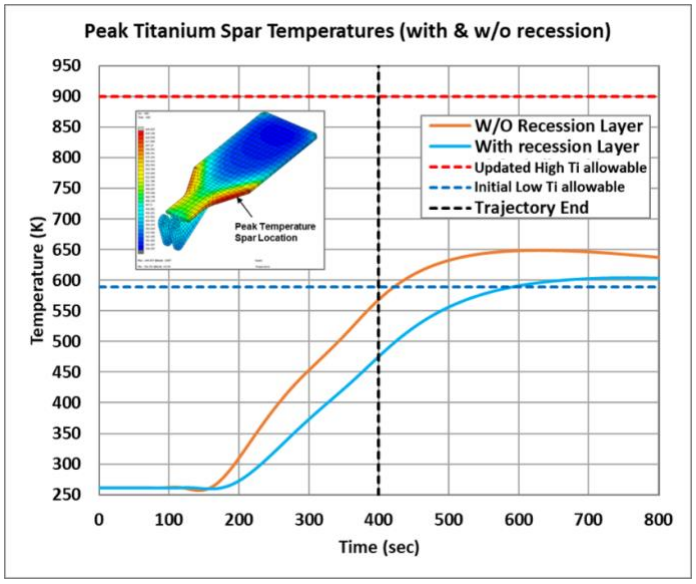

Figure 18: Titanium spar temperature histories at the peak temperature location.

V. Conclusion

Analysis was performed to build upon the findings of previous work within the Pterodactyl project. In-depth, thermal analyses for the flap control system were run on the worst-case scenario flap, Flap 3. The thermal design of the flap was first evaluated by 1D point analysis using the FIAT program. To account for the expected multi-dimensional effects, a 3D model was created and analyzed in Marc/Mentat. At the beginning of the trajectory, comparisons show that the 1D results over-predicted structure temperatures at most locations, except for locations near the spar where the additional heating at the bracket raises the titanium temperatures faster in the 3D analysis. By the end of the trajectory, all locations except the shoulder predict lower structure temperatures in the 3D analysis than the 1D due to the added thermal mass of the TPS on the aft side of the spar. The results show that the current design is within margins, at its most conservative evaluation. Many elements of the original design may be overly conservative and indicate that reductions in the TPS thickness can be made to resolve potential mechanical integration issues. For example, the lower allowable temperature limit on the spar, in Figure 18, was used for the original 1D analysis, however further structural work raised this temperature limit to a higher value, meaning the spar temperatures could be ~300K higher than they were initially designed for. In addition, the cooler titanium temperatures away from the shoulder suggest that mass could be saved by contouring the thickness of the HEEET material. Among the lessons learned from this analysis, it was primarily found that pursuit of a 3D thermal analysis is only beneficial if there are mechanical and aerodynamic challenges with integrating the flap to the heatshield. If these challenges do not exist, the prediction of the 1D thermal analysis is sufficient to envelope the maximum TPS thickness on the flap.

Acknowledgments

The authors of this paper would like to thank NASA Space Technology Mission Directorate's Early Career Initiative (ECI) program for guiding and funding this work. Specifically, the ECI Program Executive Ricky Howard and our

ECI mentor Michelle Munk. We would also like to thank our collaborators at NASA Ames Research Center: Susie Go, Ken Gee, Michael Schuh, Antonella Alunni, Breanna Johnson, Wendy Okolo, Bryan Yount, Benjamin Margolis, Alan Cassell, Don Ellerby, Milad Mahzari, Frank Milos, Owen Nishioka, and Keith Peterson.

References

[1] D'Souza, S. N., Alunni, A. I., Yount, B. C., Okolo, W. A., Margolis, B. W., Hibbard, K.E., Barton, J. D., Hawke, V., Hays, Z. B., and Reddish, B. J. (2021). Pterodactyl: System Analysis of an Asymmetric and Symmetric Deployable Entry Vehicle for Precision Targeting Using Flaps. AIAA SciTech Forum. Virtual: AIAA.

[2] Yount, B. C., Cassell, A. M., and D'Souza, S. N., "Pterodactyl: Mechanical Designs for Integrated Control Design of a Mechanically Deployed Entry Vehicle (DEV)," *AIAA SciTech 2020 Forum*, AIAA, Orlando, FL, 2020.

[3] Nikaido, B. E., D'Souza, S. N., Hays, Z. B., and Reddish, B. J., "Pterodactyl: Aerodynamic and Aeroheating Database Development for Integrated Control Design of a Mechanically Deployed Entry Vehicle," *AIAA SciTech 2020 Forum*, AIAA, Orlando, FL, 2020.

[4] Johnson, B. J., Rocca-Bejar, D., Lu, P., Nikaido, B. E., Yount, B. C., D'Souza, S. N., and Hays, Z. B., "Pterodactyl: Development and Performance of Guidance Algorithms for a Mechanically Deployed Entry Vehicle," *AIAA SciTech 2020 Forum*, AIAA, Orlando, FL, 2020.

[5] Alunni, A. I., D'Souza, S. N., Yount, B. C., Okolo, W. A., Nikaido, B. E., Margolis, B. W., Johnson, B. J., Barton, J. D., Lopez, G., Wolfarth, L. S., and Hays, Z. B., "Pterodactyl: Trade Study for an Integrated Control System Design of a Mechanically Deployable Entry Vehicle," AIAA SciTech 2020 Forum, AIAA, Orlando, FL, 2020.

[6] Hays, Z. B., Yount, B. C., Nikaido, B. E., Tran, J., D'Souza, S. N., Kinney, D. J., and McGuire, M. K., "Pterodactyl: Thermal Protection System for Integrated Control Design of a Mechanically Deployed Entry Vehicle," AIAA SciTech 2020 Forum, AIAA, Orlando, FL, 2020.

[7] Reddish, B. J., Nikaido, B. E., D'Souza, S. N., Hawke, V., and Kang, H., "Pterodactyl: Aerodynamic Modeling for a Symmetric Deployable Earth Entry Vehicle with Flaps," AIAA SciTech 2021 Forum, AIAA, 2021.

[8] Okolo, W. A., Margolis, B. W., Johnson, B. J., D'Souza, S. N., "Pterodactyl: Guidance and Control of a Symmetric Deployable Entry Vehicle using an Aerodynamic Control System," AIAA SciTech 2021 Forum, AIAA, 2021.

[9] Hays, Z. B., Hawke, V.M., Yount, D'Souza, S. N., Kinney, D. J., and McGuire, M. K., "Pterodactyl: Thermal Protection System Design for an Aerodynamic Control System," AIAA SciTech 2022 Forum (to be published).

[10] D'Souza, S. N., Okolo, W. A., Nikaido, B. E., Yount, B. C., Tran, J., Margolis, B. W., Smith, B., Cassell, A. M., Johnson, B. J., Hibbard, K., Barton, J. D., and Hays, Z. B., "Developing an Entry Guidance and Control Design Capability Using Flaps for the Lifting Nano-ADEPT," *AIAA Aviation 2019 Forum*, AIAA, Dallas, TX, 2019.

[11] Milos, F. S., Chen, Y., Mahzari, M., "Arcjet Tests and Thermal Response Analysis for Dual-Layer Woven Carbon Phenolic," Journal of Spacecraft and Rockets, Vol. 55, No. 3, May-June 2018.

[12] Y.K. Chen and F.S. Milos, "Ablation and Thermal Response Program for Spacecraft Heatshield Analysis," *Journal of Spacecraft and Rockets*, Vol. 36, No. 3, 1999, Pp. 475-483.

[13] Gage, P., Mahzari, M., Peterson, K., Ellerby, D., Venkatapathy, E., "Technology Readiness Assessment for HEEET TPS," 16th International Planetary Probe Workshop, Oxford, UK, 2019.

[14] TPSSizer, Software Package, Ver. 3.5a, NASA Ames Research Center, Moffett Field, CA 2019.

[15] CBAERO, Configuration Based Aerodynamics, Software Package, Ver. 5.3.3, NASA Ames Research Center, Moffett Field, CA 2019.

[16] FIAT, Software Package, Ver. 312, NASA Ames Research Center, Moffett Field, CA 2019.

[17] MSC.Marc and Mentat, Software Package, MSC Software Corporation, Newport Beach, CA. https://www.mscsoftware.com/product/marc

[18] Candler, G. V., Johnson, H. B., Nompelis, I., Subbareddy, P. K., Drayna, T. W., Gidzak, V. & Barnhardt, M. D. (2015). Development of the US3D Code for Advanced Compressible and Reacting Flow Simulations. *AIAA SciTech 2015*, Kissimmee, FL.